6th International Symposium on Hydraulic Structures Portland, Oregon, USA, 27-30 June 2016
Hydraulic Structures and Water System Management
ISBN 978-1-884575-75-4 DOI: 10.15142/T3600628160853

Effect of a Large Bed Roughness on Positive Surge Propagation in Canals

S.C. Yeow[1], H. Wang[1] and H. Chanson[1]
[1]School of Civil Engineering
The University of Queensland
Brisbane QLD 4072
Australia
E-mail: h.chanson@uq.edu.au

ABSTRACT

In open channels and water supply canals, the brusque operation of control valves and gates may induce large unsteady flow motions called surges. To date, the literature has focused on the propagation of surges in smooth canals, ignoring the effects of large roughness and debris. Herein, a physical study was conducted under controlled flow conditions to study the turbulent mixing in the close vicinity of a large circular bed roughness element during the upstream propagation of positive surges. Detailed free-surface and instantaneous velocity measurements were conducted with and without the large and flat cylindrical element. For a number of tests, the experiments were repeated 25 times, and the results were ensemble-averaged. The data suggested that the positive surge propagation was associated with large instantaneous free-surface fluctuations for all investigated flow conditions. The velocity measurements showed large variations in longitudinal velocity during the surge generation, as well as large fluctuations of all velocity components. The presence of the large bed element modified the velocity fluctuations and unsteady Reynolds stresses in the vicinity of the element. The present results implied the potential for bed scour around the element during surge propagation.

Keywords: *Positive surges, Large cylindrical roughness element, Turbulence, Mixing, Physical modelling, Scour.*

1. INTRODUCTION

In open channels, canals, and rivers, a rapid increase in flow depth will induce a positive surge, also called a bore or compression wave (Henderson 1966, Liggett 1994). The positive surge is a translating hydraulic jump. The shape of the bore front is characterized by its Froude number Fr_1, whose expression may be derived based upon momentum considerations for an irregular channel cross-section:

$$Fr_1 = \frac{V_1 + U}{\sqrt{g \times A_1 / B_1}} \quad (1)$$

where V_1 is the initial flow velocity positive downstream, U is the bore celerity positive upstream, g is the gravity acceleration, A_1 is the initial flow cross-section area, and B_1 is the initial free-surface width (Chanson 2012). A well-known geophysical application is the tidal bore, which is a positive surge propagating upstream in an estuarine zone when the tidal flow turns to rising, rushing into a funnel shaped river mouth with shallow waters (Tricker 1965, Chanson 2011a). Figure 1 presents photographs of tidal bores propagating upstream. Tidal bores can be dangerous, adversely impacting man-made structures and endangering lives. In recent years, the Hoogly River bore (Figure 1B) gained in strength due to the completion of upstream dams, and the tidal bore destroyed several bridge structures. The impact of a tidal bore on bridges and bridge piers is rarely documented, although some studies were conducted on the impact of the G15 Shenhai Expressway and G15W Changtai Expressway bridges over the Hangzhou Bay and Qiantang River mouth (China) (Lu et al. 2009). Another example is the 15th century Pont Aubaud bridge on the Sélune River (France) (Chanson 2011b).

To date, there is little information on the impact of man-made structures on positive surges and bores. The literature does not cover the effects of debris and large roughness. The present contribution examines in detail the propagation of positive surges over a large cylindrical roughness element, representative of a damaged bridge pier foundation.

The turbulence and turbulent mixing generated by the passage of the positive surge were carefully documented under controlled flow conditions. The experimental results showed the impact of the large element on the steady and unsteady turbulent shear stresses in the close vicinity of the element.

(A) Undular bore of the Dordogne River (France) on 29 October 2015 (Photograph Hubert Chanson)

(B) Hoogly River bore (India) in March 2015 (Courtesy of Antony Colas)

Figure 1. Photographs of positive surges in natural estuaries

2. EXPERIMENTAL SETUP, INSTRUMENTATION, AND FLOW CONDITIONS

2.1. Experimental Facility and Instrumentation

New experiments were conducted in a new 15 m long 0.5 m wide tilting flume. The bed slope was horizontal for all experiments herein. The flume was made of smooth PVC bed and glass walls. The initially steady flow was supplied by an upstream water tank, 2.0 m long and 1.25 m wide, equipped with baffles and two rows of flow straighteners, leading the water to the flume through a smooth three-dimensional convergent intake. The initial flow conditions could be controlled by a radial gate located next to the channel's downstream end (x = 14.75 m). The positive surge was generated by the rapid closure of a Tainter gate that was located at x = 14.10 m, just upstream of the radial gate (Fig. 2A). The Tainter gate closure time was less than 0.15 s to 0.2 s, and the gate closure time had no impact on surge propagation.

The water discharge was measured with a Venturi meter with an accuracy of 2%. In steady flows, the water depth was measured using rail mounted pointer gauges with an error of ±0.5 mm. The unsteady flow depths were measured with a series of acoustic displacement meters Microsonic™ Mic+25/IU/TC located at several longitudinal distances above the channel centerline: x = 6.1 m, 7.1 m, 8.1 m, 9.1 m, and 14.15 m, with an accuracy of 0.18 mm (Microsonic 2004). The instantaneous velocity measurements were performed using an acoustic Doppler velocimeter (ADV) Nortek™ Vectrino+ (Serial No. VNO 0802) equipped with a three-dimensional side-looking head. The ADV head is seen in Figures 2B and 2C. The error on the velocity data was 1% of the velocity range, herein ± 1 m/s: that is ±0.01 m/s (Nortek 2009). The acoustic displacement meters and ADV were synchronized within 1 ms and sampled simultaneously at 200 Hz. The vertical translation of ADV system was controlled by a fine adjustment traverse connected to a Mitutoyo™ digimatic unit. The error on the vertical position was less than 0.025 mm.

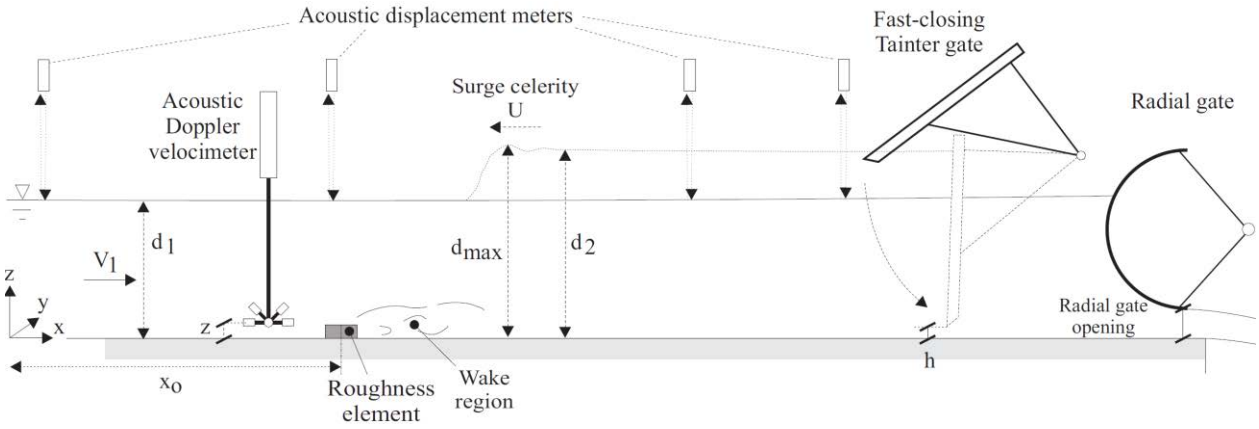

(A) Definition sketch

(B, Left) Roughness element in the dry channel looking downstream - (C, Right) Roughness element (white arrow) beneath an advancing bore - Flow conditions: Q = 0.061 m^3/s, d_1 = 155 mm at x = 5.9 m, Fr_1 = 1.39

Figure 2. Positive surge propagation in the experimental channel

2.2. Experimental Configurations

Two bed configurations were investigated. Configuration A consisted of the original smooth PVC bed. In Configuration B, a large cylindrical element was fixed to the PVC bed (Figures 2B and 2C). Its center was located on the channel centerline (y = 0) at x_o = 7.1 m. The element was made out of PVC, and its dimensions were a diameter: D = 0.060 m and a height: H = 0.020 m. Three water discharges (Q = 0.039, 0.051 and 0.061 m^3/s) were tested (Table 1). For each experiment, the positive surge was generated by the rapid closure of the Tainter gate and the surge propagated upstream as sketched in Figure 2A. The radial gate was fully opened for the breaking bore experiments; it was initially partially closed (Table 1) to raise the initial water depth d_1 during the undular surge experiment.

Several series of experiments were conducted. Series 1 included steady flow velocity measurements upstream and downstream of the large roughness element to document the effects of the element on the initially steady flow and the extent of the wake region downstream of the cylindrical element (see below). At each location, the velocity was sampled at 200 Hz for 180 s. Series 2 consisted of free-surface measurements during the propagation of positive surge. Series 3 encompassed a series of instantaneous velocity measurements during the propagation of positive surge. Both instantaneous and ensemble-average experiments were performed. For each run, the instruments were started 60 s prior to gate closure; the sampling stopped when the surge reached the upstream intake structure. For each set of ensemble-average experiments, a total of 25 runs were repeated in Series 2 and 3. The median free-surface elevations and velocity components were calculated from the total ensemble as well as the fluctuating properties. Table 1 summarizes the experimental flow conditions.

Table 1. Experimental flow conditions for unsteady velocity measurements.

Bed configuration	Q (m^3/s)	d_1 (m)	Radial gate opening (m)	Tainter gate opening h (m)	Fr_1	Surge type
A - Smooth bed	0.061	0.155	N/A	0.025	1.39	Breaking
B - Cylindrical element	0.039	0.200	0.060	0.010	1.11	Undular
		0.130	N/A	0.010	1.35	Breaking
	0.051	0.140	N/A	0.025	1.40	Breaking
	0.061	0.155	N/A	0.025	1.39	Breaking

Notes: d_1: flow depth measured at x = 6.1 m; Fr_1: surge Froude number; N/A: radial gate fully opened.

2.3. Experimental Flow Conditions

This study focused on fully-developed positive surges for which the mean properties became independent of time and space, thus independent of the generation process. Detailed velocity measurements were performed at several locations upstream of, above, and downstream of the cylindrical element on the channel centerline. Additional measurements were recorded at several transverse locations y. The initially steady flow data indicated that the flow was partially developed at x = 6.1 m upstream of the element, and the dimensionless boundary layer thickness δ/d_1 ranged between 0.5 and 0.6 depending upon the initial flow conditions.

The presence of the large cylindrical roughness element on the channel bed had an influence on the steady flow conditions. The effect was investigated in terms of the vertical distributions of time-averaged longitudinal velocity and standard deviations of the three velocity components to establish the region of influence of the roughness element. The measurements were performed upstream of, directly at, or above the element and downstream of the roughness element. Overall, the results showed that the large roughness element had little impact on the flow upstream of and at the element, except in its immediate vicinity. Downstream of the element, a wake region was observed. Typical results are shown in Figure 3, where V_x is the longitudinal velocity component, x_o is the longitudinal coordinate of the large element center, and D is its diameter. In Figure 3, the downstream half of the large element is shown with a thick, solid black line. The wake region was detected up to a distance $(x-x_o)/D < 20$, D

being the diameter of the element, with a vertical extent $z/H < 4$ where H is the height of the element, and a transverse extent $-4 < y/D < 4$.

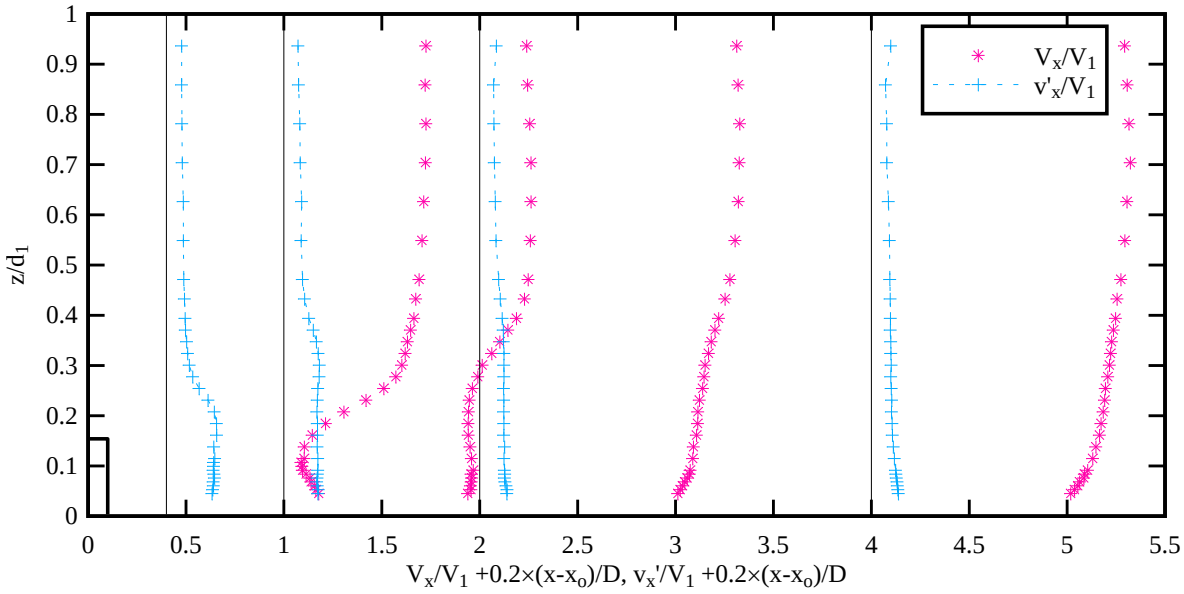

Figure 3. Dimensionless vertical distributions of time-averaged longitudinal velocity and standard deviation of longitudinal velocity downstream of the large element in steady flow - Flow conditions: Q = 0.038 m^3/s, d_1 = 0.130 m at x = 5.9 m, Flow direction from left to right

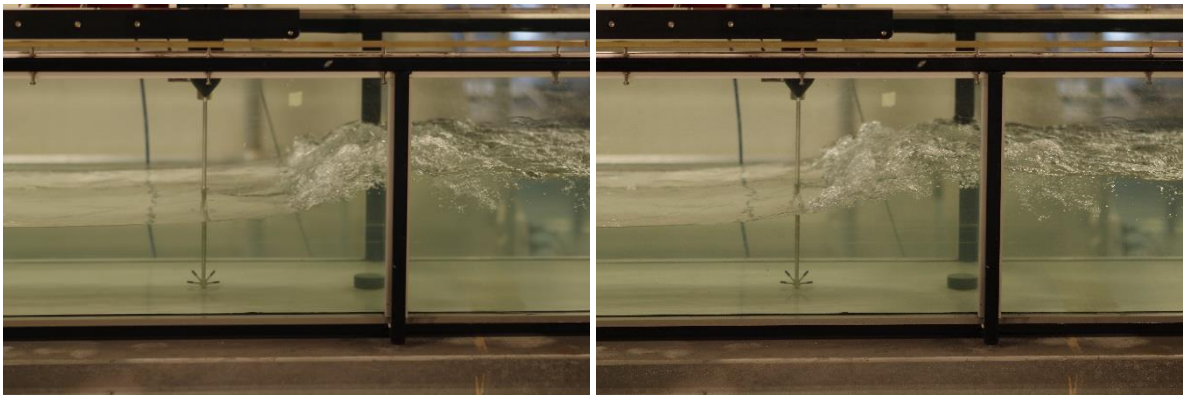

Figure 4. Positive surge propagation above the large roughness element - Flow conditions: Q = 0.061 m^3/s, d_1 = 0.155 m at x = 5.9 m, Fr_1 = 1.39, Tainter gate opening after closure: h = 25 mm - From left to right: 0.121 s between successive photographs (shutter speed: 1/400 s)

3. BASIC OBSERVATIONS

Free-surface measurements under unsteady flow conditions were conducted for three breaking and one undular bore flow condition (Table 1). The rapid gate closure generated a bore propagating upstream against the initially steady flow. Figure 4 shows a typical sequence of photographs taken during the propagation of the bore. The bore passage was characterised by a rapid rise in free-surface elevation. For $Fr_1 < 1.3$, the bore free-surface was undular: i.e., smooth with the first wave crest followed by a train of secondary undulations. For larger Froude numbers, a marked roller was observed, associated with large scale turbulence and air bubble entrainment (Fig. 4).

The free-surface properties were analyzed based upon the ensemble-average free-surface data. Quantitative results are presented in Figures 5 and 6, in terms of the ratio of conjugate depths and maximum free-surface elevation. In Figure 5, the present data compare well with the Bélanger equation as well as past experimental data in horizontal rectangular channels with smooth and rough inverts. Figure 6 presents the maximum free-surface elevation; both present data and past results are in agreement, showing an upper limit corresponding well to the criterion for solitary wave breaking (Peregrine 1966). The instantaneous free-surface fluctuations were characterized in terms of the difference between the third and first quartiles of the ensemble (d_{75}-d_{25}). The data (not shown) indicated maximum free-surface fluctuations shortly after the bore leading edge, as reported by Leng and Chanson (2016).

Both visual observations and acoustic displacement meter data showed that the presence of the large roughness element had a negligible impact on the free-surface profile and basic free-surface characteristics. As an illustration, the breaking bore data reported in Figures 5 and 6 show no distinctive difference between the two bed configurations.

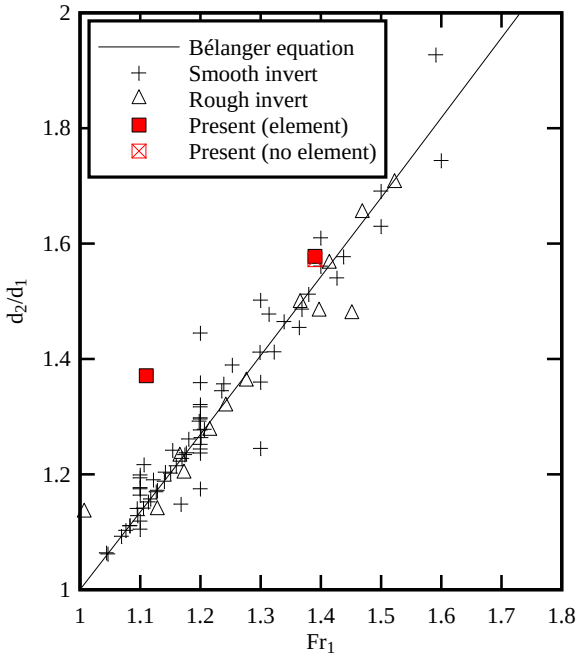

Figure 5. Ratio of conjugate depths d_2/d_1 in positive surges propagating in horizontal rectangular channels - Comparison between present ensemble-averaged data at x = 7.1 m with and without large element and laboratory data on smooth invert (Favre 1935, Treske 1994, Chanson 2010a, Docherty and Chanson 2012, Leng and Chanson 2016) and rough invert (Chanson 2010a, Docherty and Chanson 2012)

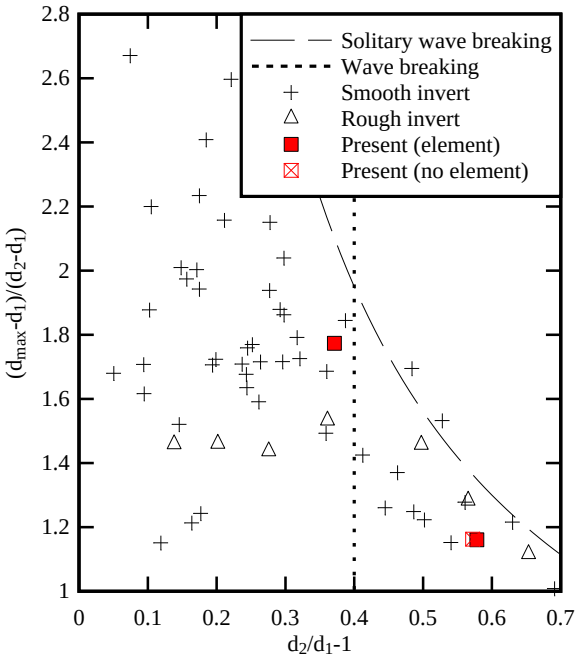

Figure 6. Dimensionless maximum water elevation $(d_{max}-d_1)/(d_2-d_1)$ in positive surges propagating in horizontal rectangular channels - Comparison between present ensemble-averaged data at x = 7.1 m with and without large element, smooth invert data (Peregrine 1966, Koch and Chanson 2008, Chanson 2010a,2010b, Leng and Chanson 2016) and rough invert data (Chanson 2010a) and solitary wave breaking onset - Dashed line indicates the onset of breaking at the first wave crest

4. VELOCITY MEASUREMENTS

All the instantaneous velocity measurements showed a sudden deceleration associated with the passage of the positive surge. The rapid deceleration phase was followed by some transient recirculation, previously reported by Docherty and Chanson (2012), Khezri and Chanson (2012), and Leng and Chanson (2016). The passage of the bore was associated with large fluctuations of all three velocity components (data not shown). In absence of large element, the results were close to those of Leng and Chanson (2016) obtained with the same discharge per unit width and comparable Froude numbers. Herein, we focus on the impact of the large roughness element on the velocity field.

The effect of the large element was tested systematically in terms of the instantaneous and ensemble-averaged velocity data for a breaking bore at several transverse locations y/D = 0, 0.5, 0.75, and 1. A typical example is presented in Figure 7, showing the time-variations of ensemble-averaged longitudinal velocity $(V_x-V_2)/(V_1-V_2)$ on the channel centerline, where V_2 is the conjugate flow velocity and all velocities are positive downstream, and t is the time from the start of data acquisition (i.e., 60 s prior to Tainter gate closure). The impact of the large element was most significant on the channel centerline for $-5 < (x-x_o)/D < +5$. First, a longer transient recirculation was observed both upstream and downstream of the element. This is illustrated in Figure 7 where d is the instantaneous water depth and the blue arrow highlights the transient circulation duration, nearly twice as long in presence of the large element. Second, the transient recirculation was characterized by stronger velocity recirculation magnitudes: that is, almost 60% larger in presence of the roughness element.

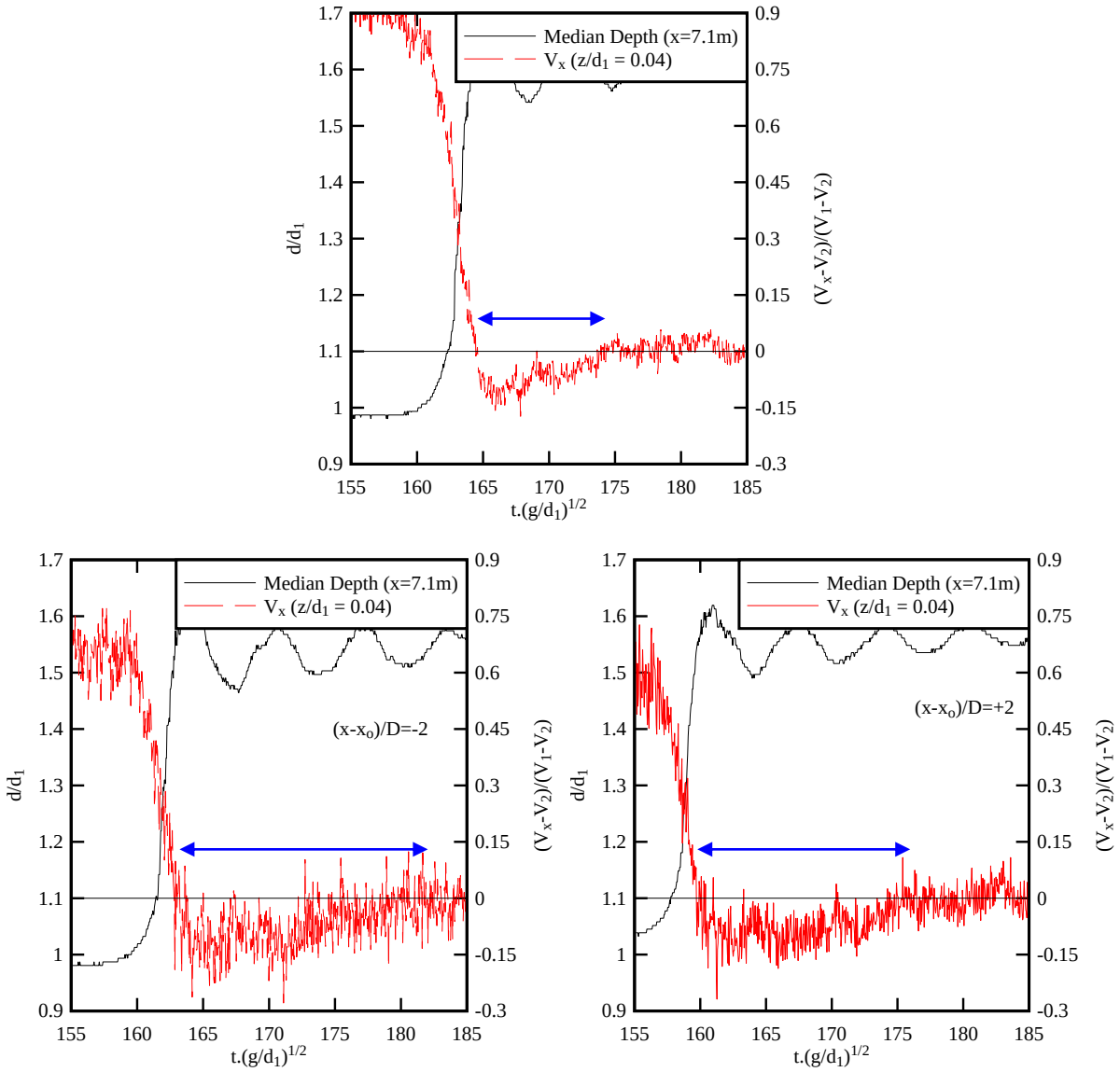

Figure 7. Time variations of ensemble-averaged longitudinal velocity: comparison between bed configuration A (no element) [Top] and bed configuration B: Bottom Left: $(x\text{-}x_o)/D$=-2 and Bottom right: $(x\text{-}x_o)/D$=+2 - Flow conditions: Q = 0.061 m^3/s, d_1 = 0.155 m at x = 5.9 m, Fr_1 = 1.39, z/d_1 = 0.04, y = 0 (centerline), Tainter gate opening after closure: h = 25 mm

Physically, the advancing positive surge first encountered the wake region downstream of the element (sketched in Figure 2A). The interactions between the wake motion and the surge turbulence induced large velocity fluctuations next to the invert, in the initially steady flow wake region. Once the surge passed the cylindrical element, a 'transient wake' developed upstream of the element. This transient wake was caused by some blockage effect induced by the large roughness element.

5. TURBULENT SHEAR STRESSES

The unsteady flow in positive surges was characterized by large velocity fluctuations that must be associated with large turbulent stresses. The turbulent Reynolds stress equals the fluid density multiplied by the cross-product of the

turbulent velocity fluctuations, $\tau_{ij} = \rho \times v_i \times v_j$ where ρ is the density of the fluid, v is the velocity fluctuation, and $i, j = x, y,$ or z. The Reynolds stress τ_{ij} is representative of the shear stress on the area $dx_i \times dx_j$ of an elementary control volume (dx, dy, dz) (Bradshaw 1971). Herein, the Reynolds stresses were calculated based on the ensemble-average velocity data following Docherty and Chanson (2012) and Leng and Chanson (2016). Measurements were performed with and without the presence of the large cylindrical roughness element. Typical results are presented in Figure 8 in terms of the median shear stresses $\rho \times v_x \times v_x$ and $\rho \times v_x \times v_y$.

The experimental results indicated that the propagation of the surge was associated with a sharp increase in Reynolds stress magnitude during the front passage (Fig. 8), together with large and rapid fluctuations in shear stresses. The maximum Reynolds stresses were typically observed after the bore arrival. The corresponding time lag was comparable with and without the roughness element and close to the findings of Leng and Chanson (2016). Overall, these patterns were observed for all Reynolds stress tensor components.

The presence of the large roughness element was mostly felt upstream of the element and around the element. Lesser effects were observed downstream of the element. Upstream of the element, the surge passage resulted in an increase in the mean normal and tangential stresses immediately upstream of the element at $(x-x_o)/D = -1$. Further upstream, only a slight increase in shear stresses was observed at $(x-x_o)/D < -2$. Around the element (i.e., $(x-x_o)=0$), its presence impacted onto the shear stress data close to the bed at $y/D = 0.75$, and 1, with larger turbulent stress magnitudes.

In open channels and water supply canals, the brusque operation of control gates may induce large unsteady flow motion called surges. Although the effects of such a rapid gate operation must often be restricted, this type of operation may be used to scour silted channels and sewers (Riochet 2008, Sun et al. 2016). The present results showed that a large roughness element may impact both steady and unsteady flow motions. During surge propagation, large shear stress levels were observed around the element that might lead to enhanced scour and bed erosion. The repetition of positive surge events could yield the development of a large scour hole surrounding the cylindrical element.

6. CONCLUSION

In open channels and canals, a sudden rise in water elevation is associated with the propagation of a positive surge. A related flow motion is a tidal bore in a small number of estuaries. To date, the literature focused on the propagation of surges in flat bed channels, and the effects of large roughness elements were un-accounted for. Herein, a physical study was performed to assess the impact of a large and flat cylindrical roughness element on the upstream propagation of positive surges.

The results showed that the large element had negligible impact on the steady and unsteady free-surface properties. The instantaneous velocity measurements showed stronger and longer transient recirculation during the bore passage immediately upstream and downstream of the element. Larger velocity fluctuations were further recorded, and the findings were associated with larger turbulent shear stresses around the roughness element. The results suggested some enhanced scour and bed erosion around the large element and the potential development of a large scour hole in mobile bed channels.

Further investigations should be conducted using mobile bed channels and could encompass both cylindrical element and cylindrical column. The latter would be representative of a bridge pier, and an important application could be the prediction of scour hole development around a pier, for example in a tidal bore affected estuary.

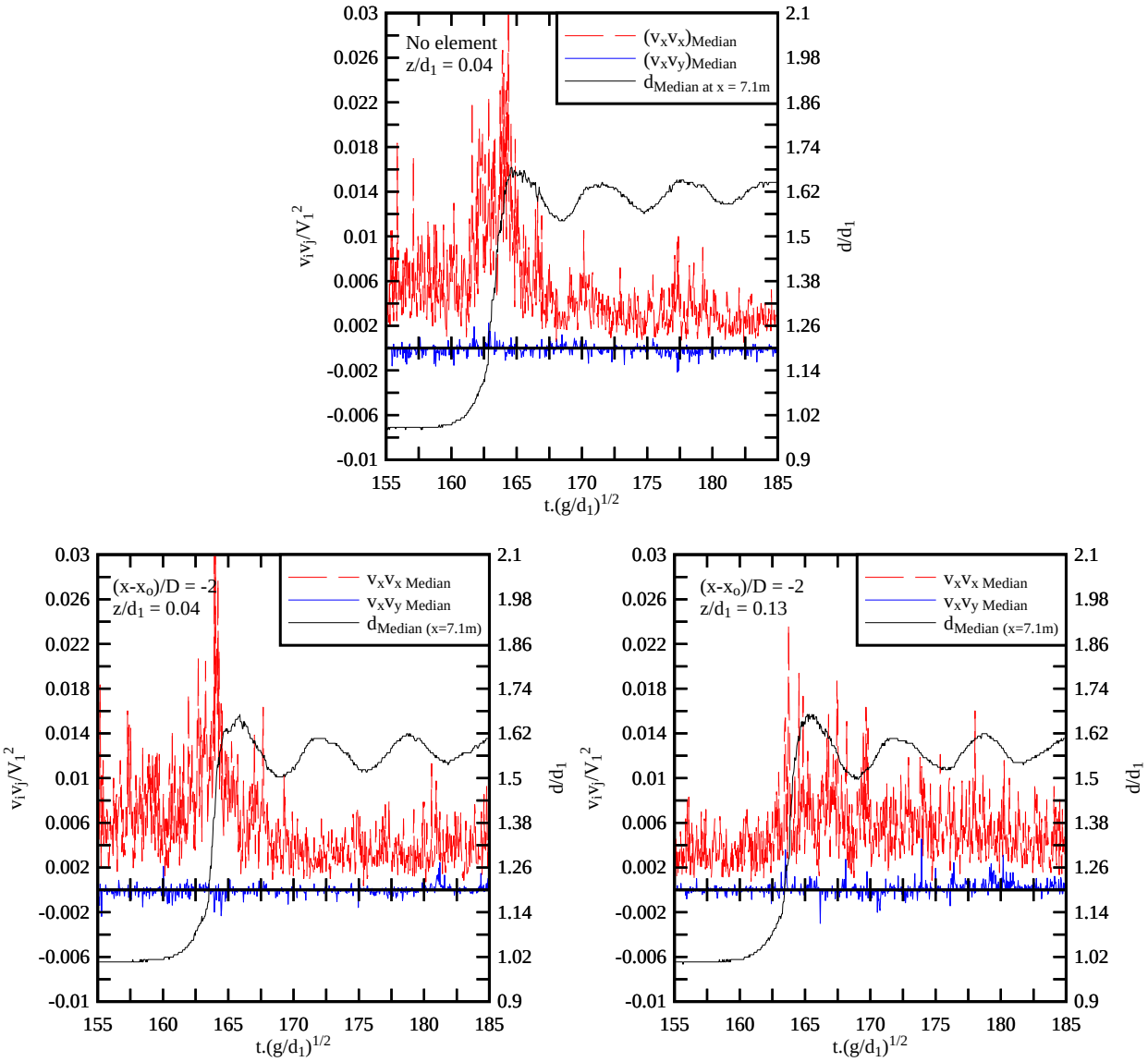

Figure 8. Time variations of ensemble-averaged Reynolds stresses $v_x v_x$ and $v_x v_y$: comparison between bed configuration A (no element) [Top] and bed configuration B [Bottom] at $(x\text{-}x_o)/D$=-2 - Flow conditions: Q = 0.061 m^3/s, d_1 = 0.155 m at x = 5.9 m, Fr_1 = 1.39, y = 0 (centreline), Tainter gate opening after closure: h = 25 mm

7. ACKNOWLEDGMENTS

The authors thank Ms. Xinqian Leng for her input and advice during the project. They acknowledge the technical assistance of Jason Van Der Gevel and Stewart Matthews (The University of Queensland). The financial support through the Australian Research Council (Grant DP120100481) is acknowledged.

8. REFERENCES

Bradshaw, P. (1971). An Introduction to Turbulence and its Measurement. Pergamon Press, Oxford, UK, The Commonwealth and International Library of Science and technology Engineering and Liberal Studies, Thermodynamics and Fluid Mechanics Division, 218 pages.

Chanson, H. (2010a). Unsteady Turbulence in Tidal Bores: Effects of Bed Roughness. Journal of Waterway, Port, Coastal, and Ocean Engineering, ASCE, Vol. 136, No. 5, pp. 247-256 (DOI: 10.1061/(ASCE)WW.1943-5460.0000048).

Chanson, H. (2010b). Undular Tidal Bores: Basic Theory and Free-surface Characteristics. Journal of Hydraulic Engineering, ASCE, Vol. 136, No. 11, pp. 940-944 (DOI: 10.1061/(ASCE)HY.1943-7900.0000264).

Chanson, H. (2011a). Tidal Bores, Aegir, Eagre, Mascaret, Pororoca: Theory and Observations. World Scientific, Singapore, 220 pages.

Chanson, H. (2011b). Undular Tidal Bores: Effect of Channel Constriction and Bridge Piers. Environmental Fluid Mechanics, Vol. 11, No. 4, pp. 385-404 & 4 videos (DOI: 10.1007/s10652-010-9189-5).

Chanson, H. (2012). Momentum Considerations in Hydraulic Jumps and Bores. Journal of Irrigation and Drainage Engineering, ASCE, Vol. 138, No. 4, pp. 382-385 (DOI: 10.1061/(ASCE)IR.1943-4774.0000409).

Docherty, N.J., and Chanson, H. (2012). Physical Modelling of Unsteady Turbulence in Breaking Tidal Bores. Journal of Hydraulic Engineering, ASCE, Vol. 138, No. 5, pp. 412-419 (DOI: 10.1061/(ASCE)HY.1943-7900.0000542).

Favre, H. (1935). Etude Théorique et Expérimentale des Ondes de Translation dans les Canaux Découverts. Dunod, Paris, France (in French).

Henderson, F.M. (1966). Open Channel Flow. MacMillan Company, New York, USA.

Khezri, N., and Chanson, H. (2012). Undular and Breaking Tidal Bores on Fixed and Movable Gravel Beds. Journal of Hydraulic Research, IAHR, Vol. 50, No. 4, pp. 353-363 (DOI: 10.1080/00221686.2012.686200).

Koch, C., and Chanson, H. (2008). Turbulent Mixing beneath an Undular Bore Front. Journal of Coastal Research, Vol. 24, No. 4, pp. 999-1007 (DOI: 10.2112/06-0688.1).

Leng, X., and Chanson, H. (2016). Coupling between Free-surface Fluctuations, Velocity Fluctuations and Turbulent Reynolds Stresses during the Upstream Propagation of Positive Surges, Bores and Compression Waves. Environmental Fluid Mechanics, Vol. 16, 25 pages (DOI: 10.1007/s10652-015-9438-8).

Liggett, J.A. (1994). Fluid Mechanics. McGraw-Hill, New York, USA.

Lu H.Y., Pan, C.H., and Zeng, J. (2009). Numerical simulation and analysis for combinational effects of two bridges on the tidal bore in the Qiantang River. Proceedings of 5th International Conference on Asian and Pacific Coasts, Singapore, Vol. 3, pp. 325-333.

Microsonic (2004). Instruction manual mic+ Ultrasonic Sensors with one analogue output. Microsonic GmbH, Germany, 3 pages.

Nortek (2009). Vectrino Velocimeter User Guide. Nortek AS, Norway, 42 pages.

Peregrine, D.H. (1966). Calculations of the Development of an Undular Bore. Journal of Fluid Mechanics, Vol. 25, pp. 321-330.

Riochet B (2008). La Sédimentation dans les Réseaux Unitaires Visitables: le Point de Vue d'un Exploitant. Proceedings international meeting on measurements and hydraulics of sewers IMMHS'08, Summer School GEMCEA/LCPC, Bouguenais, 19-21 August 2008, Larrarte F. and Chanson H. (eds), Hydraulic Model Report No. CH70/08, University of Queensland, Brisbane, pp. 11-19 (in French).

Sun, S., Leng, X., and Chanson, H. (2016). Rapid Operation of a Tainter Gate: Generation Process and Initial Upstream Surge Motion. Environmental Fluid Mechanics, Vol. 16, No. 1, pp. 87-100 (DOI: 10.1007/s10652-015-9414-3).

Treske, A. (1994). Undular Bores (Favre-Waves) in Open Channels - Experimental Studies. Journal of Hydraulic Research, IAHR, Vol. 32, No. 3, pp. 355-370.

Tricker, R.A.R. (1965). Bores, Breakers, Waves and Wakes. American Elsevier Publ. Co., New York, USA.